Optical and THz signatures of sub-cycle tunneling dynamics

T. Balciunas [a,*], A.J. Verhoef [a], A.V. Mitrofanov [a], G. Fan [a], E.E. Serebryannikov [b], M.Y. Ivanov [c], A.M. Zheltikov [b,d], A. Baltuska [a]

[a] Photonics Institute, Vienna University of Technology, Austria
[b] Physics Department, M.V. Lomonosov Moscow State University, Russia
[c] Department of Physics, Imperial College London, United Kingdom
[d] Department of Physics, Texas A&M University, USA

ARTICLE INFO

ABSTRACT

We present experimental observation of optical signals induced by tunnel ionization and a theoretical model for the generation of new optical and THz frequencies in media ionized by a high intensity laser field. The emergence of sidebands is treated as an integral part of the same underlying process of electron-plasma emission through tunneling. First, investigating the broadly transparent case of gaseous media, we demonstrate the ability to detect multiple new frequency components in the probe field direction, and describe in detail how such tunnel-ionization induced signals can be reliably separated from concomitant nonlinear responses. Second, we apply the same pump–probe method to transparent dielectrics, thus expanding the field of attosecond physics to systems where direct detection of charged particles is unfeasible. Third, we show that a probe beam with a central frequency tuned close to the half of the pump frequency acquires a tunable sideband with a frequency close to zero.

© 2013 Published by Elsevier B.V.

1. Introduction

With the invention of the laser in the 1960s and subsequent achievements in ultra-short pulse generation, light fields with electrical field strength of several volts per Angstrom have become routinely available. An electric field of this strength can significantly modify the atomic potential seen by outer valence electrons, allowing their release from atoms, molecules and solids. Liberation of an electron by the laser field from its bound atomic state is the primary step in strong field – matter interaction.

In his revolutionary theoretical paper [1], Keldysh showed that ionization in strong infrared laser fields can proceed via a mechanism similar to tunneling: a valence electron can escape the binding potential through the barrier modified by a strong laser field. Typically, the tunneling ionization (TI) regime is defined to occur when the Keldysh parameter γ:

$$\gamma = \frac{\omega_L \sqrt{2 m_e I_p}}{|e| E_0} \tag{1}$$

is much less than unity $\gamma \ll 1$ (ω_L – laser carrier frequency, E_0 – amplitude of the electric component of the light field, I_p – ionization potential of an atom, m_e and e – electron mass and charge respectively). In a later theoretical work [2] Yudin and Ivanov suggested that tunneling remains significant even for γ greater than one.

The case of $\gamma \sim 1$ corresponds to the non-adiabatic tunneling regime. Since in this regime the corresponding tunneling time is on the order of the optical half-cycle, the potential barrier formed by the atomic field and oscillating laser field varies during tunneling.

In the regime of TI, the probability of ionization is extremely sensitive to the amplitude of the electric field: only a sufficiently strong field can cause substantial modification of the binding atomic potential. This sensitivity has two consequences. First, tunneling reaches its maximum near the peaks of the electric field, and hence ionization is predicted to be confined to short intervals of time, lasting a fraction of a half cycle of the light field oscillation. Second, the ionization rate becomes strongly sensitive to the carrier-envelope phase of the light pulse. Consequently, one expects the ionization yield to have a step-wise profile on a sub-femtosecond time scale, where each step is locked to a half-cycle of the laser field. Such a behavior of the ionization yield has been recently visualized in an elegant time-of-flight spectrometry measurement [3] where the attosecond steps in the ion yield were detected using an isolated soft X-ray attosecond pump pulse and a few-cycle optical probe. It also demonstrates that the tunneling regime of ionization remains significant even at γ values greater than unity (as it was predicted in [2]) since $\gamma \sim 3$ was used in the experiment.

It is important to emphasize that direct observation of ions was performed in [3] using time-of-flight measurement. This technique implies the detection of charged particles (electrons or ions) that have escaped the interaction volume. It is successfully used in attosecond physics [4,5] to study different intra-atomic and

* Corresponding author.
   E-mail address: tadas.balciunas@tuwien.ac.at (T. Balciunas).

intra-molecular process in the gas phase [6] and on solid surfaces [7]. However, it cannot be used to study ionization processes in the volume of bulk materials. For such materials, one has to develop another method, not based on direct detection of ionization products.

Recently, we have devised an all-optical approach for investigation of ionization dynamics in transparent media, based on the detection of a time-resolved optical signal which uniquely originates from the electron tunneling [8]. This method utilizes a non-collinear optical pump–probe scheme, where ionization dynamics created by a few-cycle pump pulse is read out by a probe pulse in the form of new spectral components. The non-collinear pump–probe scheme allows us to discriminate between the pump–probe delay-dependent signal in the direction of the probe pulse, originating from ionization, and all possible signals generated through the nonlinear response of the medium.

From the dynamics of TI, confined to a small fraction of each laser half-cycle and hence implying rich harmonic content, one naturally expect that new frequencies are generated by the ionization process. These frequencies should be spaced by twice the optical frequency of the ionizing pump field. The generation of high harmonics associated with the tunnel ionization was first proposed by Brunel [9]. Although later it was shown by Corkum [10] that HHG in gases is better explained by the recombination of the accelerated electrons after TI (see also Fig. 1), investigation of harmonic generation following the mechanism proposed by Brunel can offer more insights in the dynamics of TI in the adiabatic and non-adiabatic regimes.

In the pump–probe scheme, it is not required that the pump and probe fields have the same frequency. Thus one may expect that the ionization profile read out by the probe field gives rise to sidebands separated by twice the optical frequencies of the pump field with respect to the frequency of the probe field. When the polarization of the probe field is the same as the polarization of the pump field, and the fields propagate together in the same direction, the modulation on the pump field caused by the probe causes a modulation of the ionization rate, which results in the generation of even more frequencies. The implications of this insight are reviewed in Fig. 2.

Here we present experimental results on optical signals induced by TI, detected in different frequency ranges, and a theoretical model of the generation of new optical frequencies in media ionized by a high-intensity laser field. After the presentation of a semiclassical framework to describe TI in a multicolor laser field and a quantum mechanical interpretation, we present different experiments supporting our model. First, we demonstrate using TI in gaseous media that our noncollinear pump–probe scheme allows detecting the new frequency components in the probe field direction, such that the TI induced signal can be separated from other nonlinear responses. Second, we show that the method allows detecting the TI induced signal from bulk dielectric media, expanding the field of attosecond physics to systems where direct detection of charged particles is impossible.

When the probe beam has the same polarization as the pump, and has a frequency close to half the pump frequency, TI can be suppressed for every other half-cycle, similarly to the case when the probe frequency is close to the second harmonic of the pump [11]. In such a case, Ref. [12] showed that, in gaseous medium and adiabatic tunneling regime, the spectrum of the probe field acquires a sideband with frequency close to zero. Such a scheme offers great perspectives for broadband and high peak amplitude THz-pulse generation. We show that the frequency of the THz sideband can be continuously tuned by tuning the frequency ratio of the two color field. Our experimental observations are in good agreement with calculations of the optical response from the ionized medium using semiclassical two-step model. Finally, we show that the directional current in gases induced by incommensurate frequency fields can be directly detected. A classical description
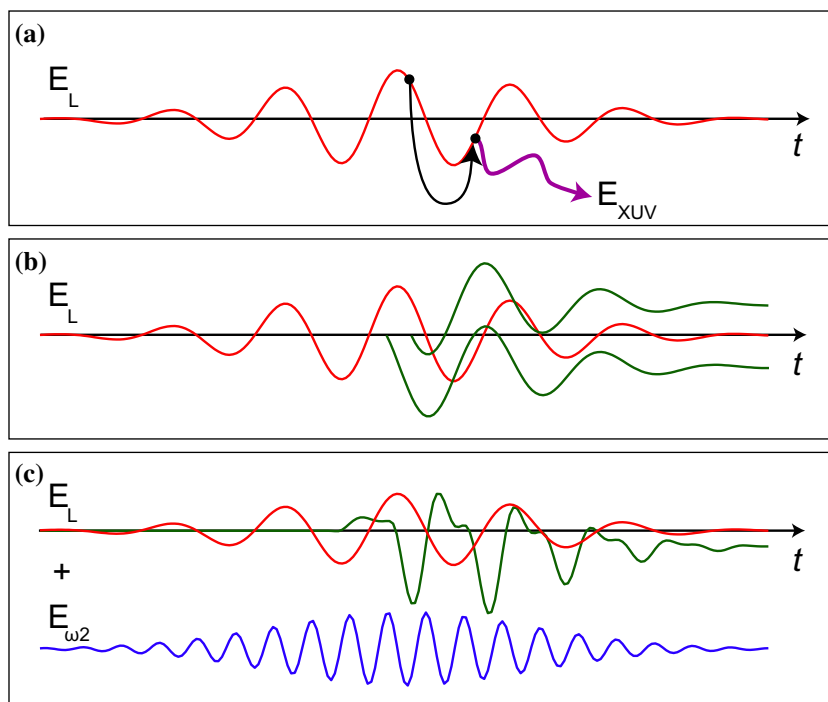
Fig. 1. Ionization in a strong laser field can be viewed as tunneling through a barrier formed by the addition of potential slope caused the laser electric field and the atom's Coulomb potential. After ionization, the motion of the freed electron is forced by the laser's electric field, and thus the freed electron can come back to its parent ion with a high kinetic energy and recombine. Upon recombination a high energetic photon is emitted (a). However, the recombination probability is low, and thus most freed electrons remain and gain energy until the laser pulse has passed (b). Generally, the electron emission is symmetric with respect to the laser polarization direction. This symmetry can be broken by adding a second laser field with an appropriately chosen different color and phase (c). The asymmetric electron emission can give rise to emission of a strong low-frequency (THz) pulse.
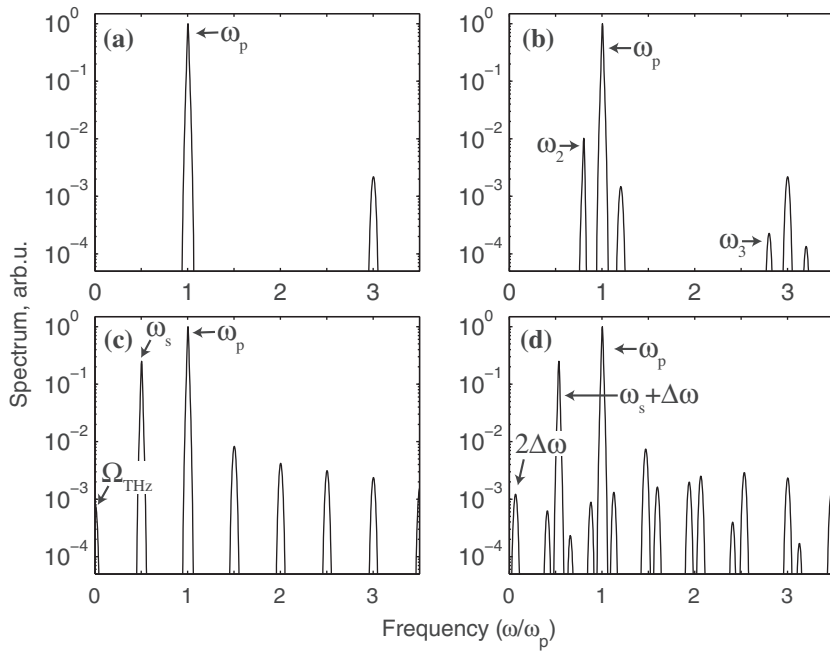
Fig. 2. Sideband generation due to tunnel ionization effects. In a monochromatic laser field, due to tunnel ionization, odd-order harmonics are generated (a). When a weak second laser field is added with a slightly different frequency, sidebands spaced by twice the stronger laser field's frequency are generated relative to the weak field's frequency as well (b). When the weak laser field's frequency is equal to half the frequency of the strong field, the tunnel ionization is enhanced every other half-cycle of the strong field. The induced asymmetric emission gives rise to sidebands spaced by exactly once the frequency of the strong field, and thus a field with almost zero frequency, i.e. THz emission can be observed as well (c). By tuning the weak field's frequency away from ½ the strong field frequency by $\Delta\omega$, the frequency of the generated THz sideband is shifted by $2\Delta\omega$ (d).

of the electron current following TI in a multi-color laser field can at the same time accurately describe the electron kinetic energy spectrum, and the generation of new frequencies from an ionized medium. We also show that the low energy electron spectrum may be used for a more robust carrier-envelope phase detection scheme, since the electron yield at low kinetic energies is orders of magnitude higher than at high kinetic energies.

2. Theoretical background

2.1. Semiclassical model of electron emission and sideband generation in a two-color field

The semiclassical model of Brunel harmonic emission [9] provides an intuitive description of the mechanism of the process. It is based on microscopic electron current production in a field. Brunel proposed a model initially aiming to explain high order harmonic generation. More recently it was shown that the superposition of two colors, namely fundamental frequency and the second harmonic of the laser field, induces a directional current and the model is used to explain the strong THz pulse emission in plasma [13]. In the high-intensity regime, the ionization of atoms or molecules can be described as a tunneling of an electron through the barrier into the continuum. Quantitatively, this is calculated using the ADK tunneling rate formula [16]. After the electron is released into a continuum, it is treated as a classical particle and is accelerated in a laser field. The velocity v_d of an electron in a laser field $E(t)$ is given by:

$$v(t) = \frac{q_e}{m_e} \int_{t_0}^{t} E(t')dt' \tag{2}$$

The resulting laser-field induced electron current density is then calculated by integrating:

$$J(t) = \frac{q_e^2 \rho}{m_e} \int_{-\infty}^{t} dt_i \Gamma(t_i) \int_{t_i}^{t} dt' E(t') \tag{3}$$

where Γ is the tunneling rate, ρ is the density of gas, q_e and m_e is the charge and mass of an electron. The emission of electromagnetic field is related to the acceleration of the charge and is therefore proportional to the derivative of the induced current density $J(t)$:

$$E_{THz} \propto \frac{dJ(t)}{dt} \tag{4}$$

2.2. Quantum mechanical treatment of Brunel emission

The classical interpretation of the emission by the induced electron current although intuitive, is not rigorous and does have serious limitations. On the other hand, full ab initio numerical integration of the time-dependent Schrödinger equation performed to calculate THz emission [14,15] shows good agreement with the experimental data. Initial steps were done to apply a strong field approximation for the calculation of the THz emission using analytical quantum mechanical model [15]. Here we show that there is a bridge between the classical model of the emission due to strong field ionization, followed by the charge motion in the laser field, and the contribution of the free–free transitions to the high harmonic emission in the quantum mechanical interpretation.

The semiclassical treatment by Brunel is based on several approximations. First, only the interaction of the free electron with the laser field is considered, the Coulomb potential of the core is neglected. The model describes the electromagnetic wave emission that arises from the current J induced by the laser field. The emitted electric field is proportional to the derivative $\dot{j}$ which is can be expressed as a product of the ionization rate and the laser field:

$$\dot{j} \propto E_L(t)n(t) \tag{5}$$

where $E_L(t)$ is the laser electric field and $n(t)$ is the time-dependent electron density. In the limit of small depletion and strong field re-

gime the free electron density can be expressed as $n(t) = N \int^t \Gamma(t') dt'$, where N is the density of the atoms or molecules and $\Gamma(t)$ is the static ionization rate. From the quantum mechanical perspective, the induced dipole moment is:

$$d(t) = \langle \psi(t) | d | \psi(t) \rangle \qquad (6)$$

The wavefunction of the whole system can be separated into continuum and bound wavepacket parts $\psi = \psi_b + \psi_c$. Similar to the semiclassical model, let us consider only the free electrons and replace the full wavefunction with the continuum wavepacket ψ_c. The derivative of the current $\dot{J}$ is associated with the second derivative of the dipole moment:

$$\ddot{d}(t) = \langle \psi_c(t) | F_{total} | \psi_c(t) \rangle \qquad (7)$$

where F_{total} is the total field acting on the electron wavepacket, which can be separated into two parts: $F_{total} = F_L + F_{core}$. The first term corresponds to the force acting on the electron by laser field and the second term is the force due to interaction with the core. Using exactly the same approximation as F. Brunel and neglecting the interaction of the liberated electron with the core, the dipole acceleration becomes:

$$\ddot{d}(t) = F_L \langle \psi_c(t) | \psi_c(t) \rangle \qquad (8)$$

The right hand side of the equation is just a probability of ionization times the force of the laser field $F_L W_C(t)$. Since $n(t) \approx N W_C(t)$, we see that the expression (8) is essentially the same as the derivative of the electron current (5) in the semi-classical treatment, which means that the emission mechanism proposed by Brunel arises due to continuum–continuum transitions.

3. High-frequency sidebands in gas targets

We experimentally observe the emission of new optical frequency components that are generated following the emission mechanism proposed by Brunel. In a non-collinear pump–probe setup, using 250 µJ, 5 fs horizontally polarized pump pulses, and 1 µJ, 10 fs vertically polarized probe pulses, we have measured the ionization induced high-frequency sidebands as a function of delay between the pump and probe pulses. In a first experiment, we have used krypton at a neutral gas pressure of ~250 mbar, and we have observed the TI induced sidebands lying around the 3rd, 5th and 7th harmonic of the pump and probe pulses. The measured spectrally resolved signals as a function of pump–probe delay are shown in Fig. 3(a). The temporally integrated signals [Fig. 3(b)] are compared with the signal obtained from numerical simulations, that includes gas and plasma dispersion, diffraction, spatial self-action induced by Kerr-nonlinearities, spectral transformation phenomena such as self phase modulation, wave mixing and harmonic generation, as well as ionization induced loss and plasma related nonlinearities. Although the signal-to-noise ratio of the experimental data is rather small, several very important agreements between the experimental data and the numerical simulations can be identified. In Fig. 3(b), the experimental data integrated along the delay-axis are compared to the full numerical results (dashed colored curves) and with the results when no propagation effects are taken into account (black dotted curves). A clear frequency shift away from 'pure' harmonics can be observed when the propagation effects are taken into account. This shift is also observed in the experimental data, although its magnitude is different for different sidebands.

In order to further investigate the TI induced sideband generation, we have performed a more extensive study of the sideband around the 3rd harmonic of our pump and probe pulses. In this study, an argon target was used. The ionization yield from argon is lower than from krypton, hence one can also expect the sideband signal to be lower. However, we use the spectrometer that is optimized for detection of light between 200 and 400 nm, so that the signal-to-noise ratio for these measurements is much higher than for the measurements using krypton, as can be seen in Fig. 4. We have investigated the influence of the pump pulse chirp on the measured signal [Fig. 4(b)], as well as the influence of the probe energy [Fig. 4(c)]. For the latter, a linear dependence of the TI induced signal on the probe energy is observed, as may be expected since the probe pulse reads out the modulation induced by the pump pulse.
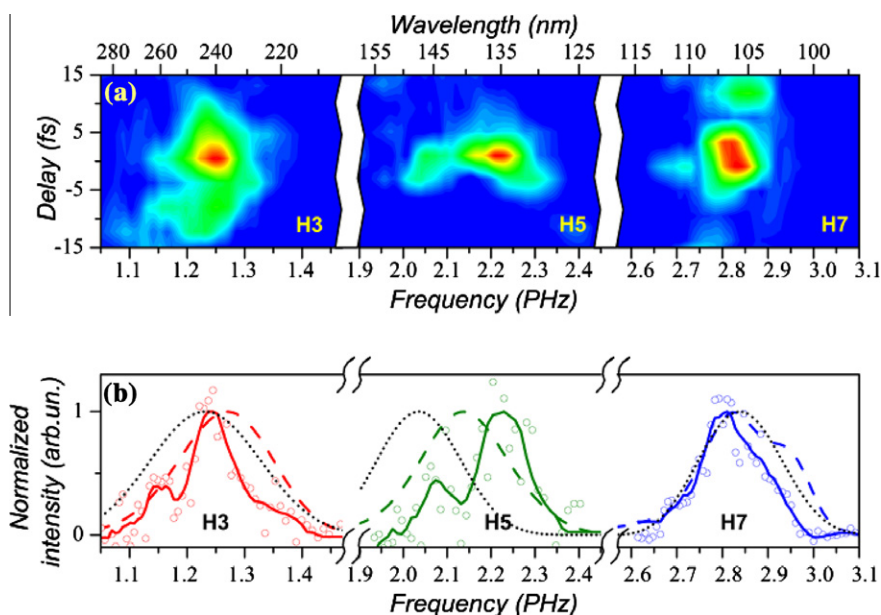
Fig. 3. High frequency sideband generation in krypton. Panel (a) shows the measured spectrally resolved signals as a function of the delay between the pump and probe pulses. In panel (b) we compare the measured signals integrated along the delay axis with the results from numerical simulations, taking into account all propagation effects (dashed colored curves) and without taking into account propagation effects (black dotted curves). The frequency shift caused by propagation effects is clearly seen in the numerical results as well as in the measured data.
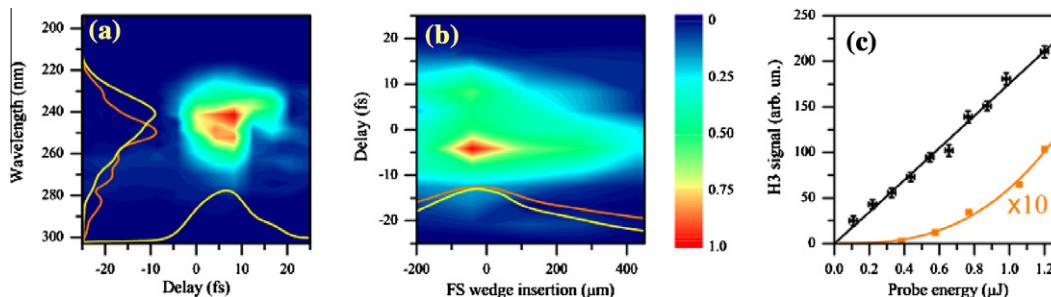
Fig. 4. Investigation of the sideband close to the 3rd harmonic frequency due to tunnel ionization in argon. Panel (a) shows the spectrally resolved measured signal as a function of pump–probe delay. The yellow curves show the signal integrated along the delay and wavelength axes. The orange curve shows the normalized third harmonic of the probe pulse measured in absence of the pump pulses. Panel (b) shows the spectrally integrated signal as a function of net material insertion in the pump beam path. The induced chirp lowers the peak intensity, and thus the ionization yield and yield of the ionization induced sideband. The yellow curve shows the normalized integrated signal, and the orange curve shows the estimated normalized peak intensity of the pump pulses. Panel (c) shows the dependence of the sideband signal on the probe pulse energy. The orange curve shows the signal in absence of the pump pulse. (For interpretation of the references to colour in this figure legend, the reader is referred to the web version of this article.)
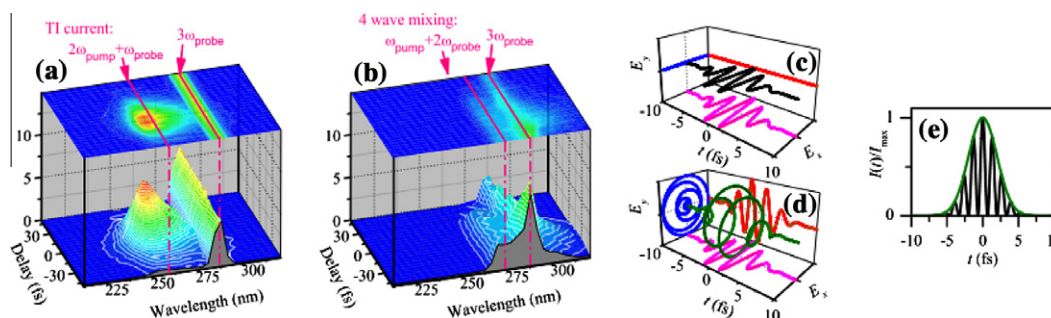
Fig. 5. Tunnel ionization induced sideband generation in a bulk dielectric (fused silica). Since the tunnel ionization rate strongly depends on the instantaneous field strength, the ionization rate in a linear polarized field peaks strongly once per half-cycle. In a circular polarized field, the tunnel ionization rate varies smoothly along the laser pulse, since the field strength never becomes zero. Panel (a) shows the tunnel ionization induced sideband generated from fused silica with linear polarized pump pulses. The signal is observed when the pump pulses have circular polarization (b). In this case, the 4-wave mixing signal $w_{pump} + 2w_{probe}$ is not blocked by the polarizer before our spectrometer, and can be used to confirm that the spatial and temporal overlap of the pump and probe pulses is not lost. Panels (c) and (d) show the temporal evolution of a respectively linear and circular polarized few cycle pulse. Panel (e) shows the normalized instantaneous intensity for the pulses shown in panels (c) (black) and (d) (green). (For interpretation of the references to colour in this figure legend, the reader is referred to the web version of this article.)

Turning to the influence of the chirp of the pump pulse on the measured signal, one can expect several effects. First, since the periodicity of the ionization steps is disrupted, spectral broadening of the TI induced signal may be expected. Second, since the pump intensity is reduced by introducing the chirp, the TI induced signal should also be reduced. In the experiment, we do indeed observe spectral broadening when small amounts of chirp is introduced. However, fast decrease of the TI induced signal with increasing the chirp makes quantitative study of the spectrally resolved signal rather complicated. Therefore we only plot the spectrally integrated TI induced signal as a function of the pump pulse chirp, which clearly shows the expected rapid decrease of the signal [see Fig. 4(b)].

4. High-frequency sidebands in bulk dielectrics

Having proved the conceptual point about the optical detection of the TI induced signal in gas targets, krypton and argon, we have subsequently performed measurements of the TI induced sideband in the wavelength range from 200 to 300 nm from different bulk dielectrics. Since in many cases the third harmonic generated by the probe beam alone was comparable in strength to the TI induced signal, we have set the central wavelength of the probe pulses to be different from the central wavelength of the pump pulses. This ensures that in addition to the spatial separation of the TI induced signal from other processes, the TI induced signal

can be spectrally separated from signals due to other processes that propagate in the same direction as the probe beam. In order to confirm that the spatial and spectral separation works, we have measured the signal with linear polarized pump pulses, as well as with circular polarized pump pulses. In the case of circular polarization, while TI can still be the dominant mechanism for ionization, the free electron density will not increase stepwise (as is the case with linear polarized pump pulses), but smoothly. Thus, in the case of circular polarized pump pulses, no sidebands will be generated. Fig. 5 shows the measured signal for the case of linear polarized pump pulses (a) and circular polarized pump pulses (b). While the absence of the TI induced sideband in the case of circular polarized pump pulses is notable, one can observe a clear signal due to 4-wave-mixing (FWM) ($\omega_{pump} + 2\omega_{probe}$) as well. While this signal does not propagate in the same direction as the probe beam, however, of all FWM signals possible it propagates closest to the probe beam, and therefore is not completely suppressed by our spatial filtering. It has to be noted, that since the signal at $\omega_{pump} + 2\omega_{probe}$ inherits its polarization from the pump pulses, it is blocked by the polarizer in our setup in the case of linear polarized pump pulses, and that in the case of circular polarized pump pulses, it has a nonzero projection on the probe polarization direction.

Since the ionization rate depends exponentially on the binding potential of the material under investigation, we have performed measurements of the TI induced sideband from different dielectrics, each with a different bandgap (binding potential). For
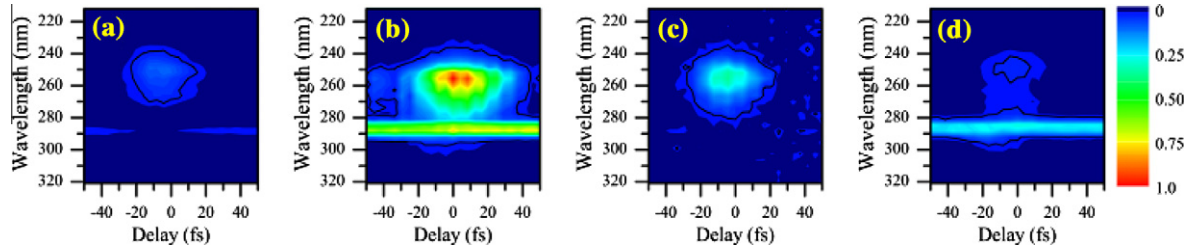
Fig. 6. Tunnel ionization of the first tunnel ionization induced sideband observed from different bulk dielectrics. (a) Soda lime silicate – Na_2O (22%) CaO (3%) SiO_2 (75%) – bandgap 6.5 eV. (b) Fused silica – bandgap 9 eV. (c) CaF_2 – bandgap 10 eV. (d) MgF_2 – bandgap 11 eV.

constant pump pulse intensity, a stronger signal is expected from materials with a smaller bandgap. In Fig. 6 we show the measured signal from different bulk dielectric materials at a pump pulse intensity of ~20 TW/cm². The expectation of a weaker signal from a material with higher bandgap is confirmed by these measurements, with the exception of the signal measured from our composite glass soda lime silicate. It has to be noted that it is known that in addition to the size of the band gap, the presence of impurities in the sample under investigation may play a significant role in suppressing or promoting ionization in the laser field. For example, samples with impurities are known to be more prone to optical damage than very pure samples of the same material. Additionally, for crystalline materials the orientation of the crystal axes with respect to the laser polarization can influence ionization as well [17].

5. Low frequency sideband generation from gas

In this section we show that the same ideas that were behind the odd-harmonic generation experiments in Sections 3 and 4 can be seamlessly extended to explain the emission of low-frequency sidebands in the THz range. In fact, the process can be treated as a special case of wavemixing based on transient nonlinearities and as suggested in Ref. [18] can lead to the emission of THz "Brunel sidebands". Mixing the fundamental field with its second harmonic breaks the symmetry of the cycle and yields emission of the even harmonic emission in additional to the odd harmonics. In addition to even high order harmonic generation, this was exploited for the generation of THz pulses in plasma by Cook and Hochstrasser [19].

There exist several interpretations of the process. Originally, the emission of the strong THz transients was attributed to a four wave mixing in air. Later, however, it was shown that the THz emission directly relies on the production of laser induced plasma. Another more accepted interpretation is a semi-classical two-step model. The second color acts as an "AC bias" by breaking the symmetry of the optical cycle and yields production of directional electron current. This directional electron burst was directly observed by means of ATI spectroscopy [20].

The experiments on the THz generation that have been performed so far were based on the degenerate scheme, where the fundamental laser field and its second harmonic are mixed. Here we use a different scheme based on generating the second field via parametric amplification. The frequency of this field can now be continuously tuned at around the degeneracy point. The frequency of the signal wave of the degenerate OPA is half the frequency of the fundamental laser pulse. This $\omega_p + \frac{1}{2}\omega_p$ scheme is similar to the popular $\omega_p + 2\omega_p$ scheme based on the second harmonic generation, except that the lower frequency component is now weaker. When the frequency of the second field is detuned from the degeneracy point, the drift of the electrons in the laser induced plasma is modulated in time, which shifts the emission peak towards higher frequencies.

An important difference in the case of multi-color pulse superposition using optical parametric amplifier (OPA) as compared to the second harmonic generation case is the phase relation between the constituent colors. In the general case, the superposition of frequency ω and $\alpha\omega$ fields can be written as follows:

$$E = E_1 \cos(\omega t + \varphi_{CEP}) + E_2 \cos(\alpha\omega t + \beta\varphi_{CEP} + \varphi_{rel}) \qquad (9)$$

In second harmonic generation both the carrier frequency and the carrier envelope phase (CEP) are doubled ($\alpha = \beta = 2$). In this case the slip of the CEP causes the delay $\tau = \varphi_{CEP} \cdot \omega^{-1}$ of the waveform with respect to the envelope, where ω is the laser frequency. Therefore, the change is unimportant if the pulse contains many cycles and the effect of the envelope on the cycle is negligible.
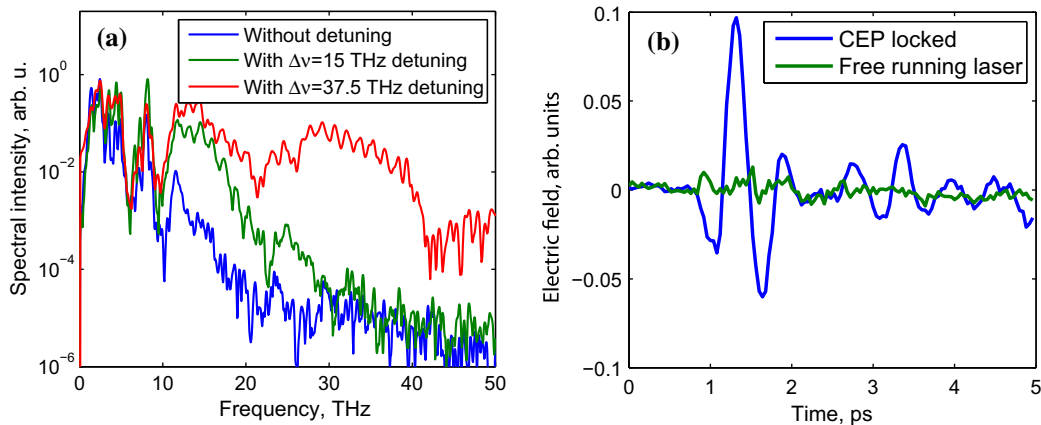

Fig. 7. (a) Emission spectrum of plasma excited with ω and $\frac{1}{2}\omega + 2\pi\Delta\nu$ fields, where $\Delta\nu = 2\upsilon_s - \upsilon_p$ is the detuning frequency. The two-color driving laser field is comprised of the fundamental wave (λ_p = 1.03 µm, 250 µJ) and a tunable signal wave generated in an OPA (λ_s = 2.06–1.8 µm, 20 µJ). (b) A comparison of the measured THz transient with the CEP of the laser locked and free running.

More generally, in the case of sum frequency generation or *n*th harmonic generation, the CEP and the frequency multiplier are the same ($\beta = \alpha = n$). Denoting $\omega t + \varphi_{CEP} = \omega t'$, we see that (i) the CEP slip only causes a shift of the waveform under the envelope, and (ii) this shift is common for both waveforms. The relative phase between the two colors is preserved.

However, in the case of an OPA seeded by a white light super continuum, the CEP of the seed pulse is preserved during parametric amplification ($\beta = 1$). Therefore, the relative phase between the two colors is affected by the CEP slip of the seed pulse, leading to extreme sensitivity of the two-color ionization dynamics to the CEP. In order to get a reproducible field shape, we need to actively stabilize the CEP of the pump and signal pulses of the OPA. Since the seed for the signal pulse is derived from the pump pulse, it is enough to stabilize the CEP of the driving laser in order to get all the waves of the OPA phase-locked together. The multi-color waveform synthesis using an OPA has the additional advantage that the frequency ratio α can be tuned continuously. The previously mentioned modulation of the electron burst emission direction in time leads to the shift of the sidebands in the frequency domain, including the lowest frequency THz sideband, as illustrated in Fig. 2.

Tunable THz emission from a plasma was generated using two colors from an OPA, which was pumped by an actively CEP stabi-
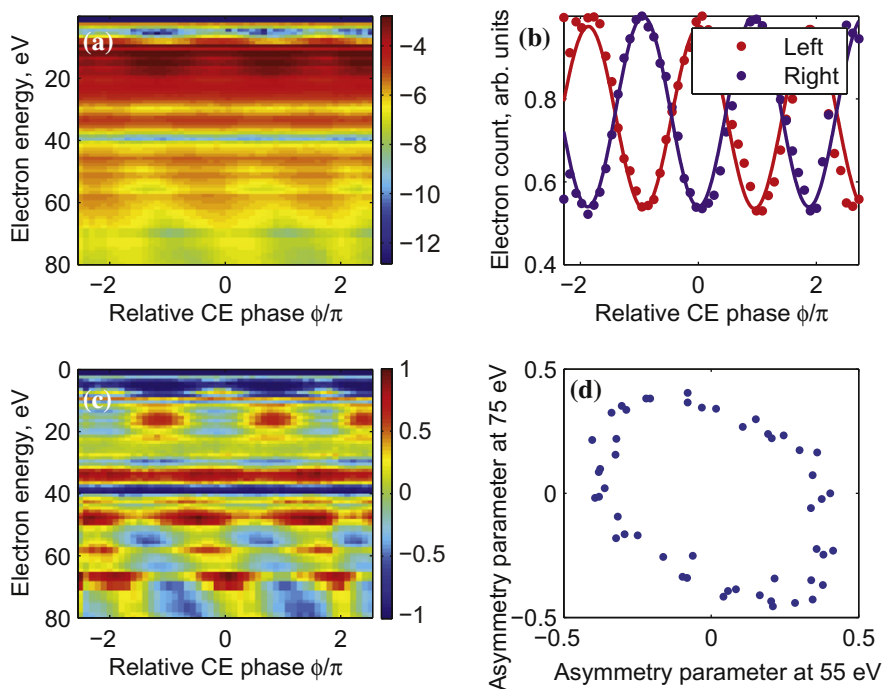
Fig. 8. ATI electron spectrum measurement. (a) Phase dependent spectrum of the electrons emitted to the right, (b) lineout at 15 eV of the left and right energy spectra for different CEP phases, (c) measured asymmetry parameter dependence on CE phase and electron energy, (d) CEP phase ellipse obtained from assymetry parameters at 55 and 75 eV energy.
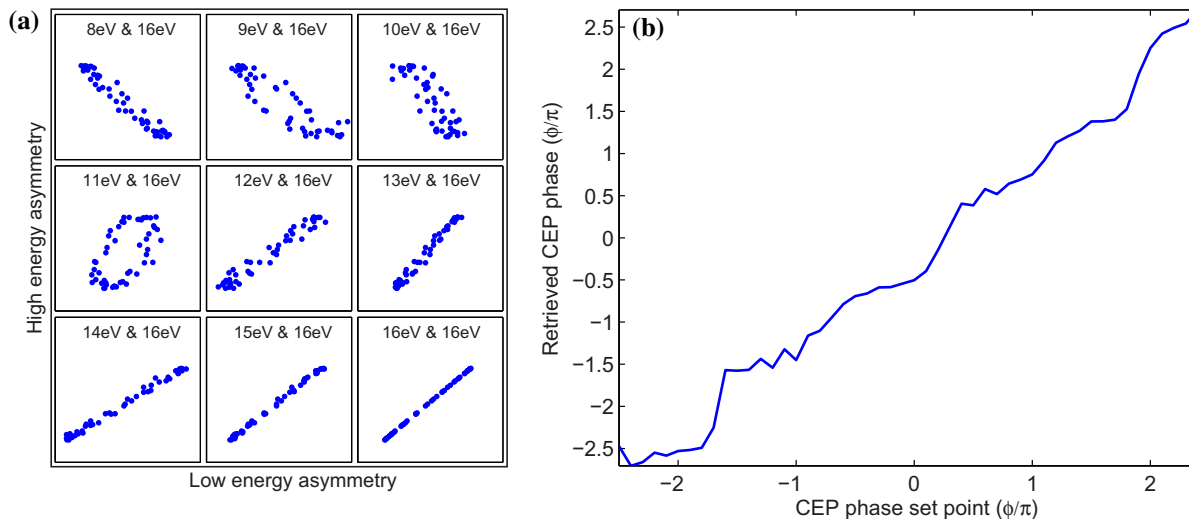
Fig. 9. Phase ellipses obtained by taking lineouts at different positions of the spectrum in the low energy range that is dominated by the direct electrons. The retrieved phase on the right hand side is obtained using 11 eV and 16 eV energy windows.

lized Yb laser. The measured spectra for different signal and pump pulse frequency ratios are shown in Fig. 7. By detuning the OPA from degeneracy the frequency of the THz sideband can be shifted up to 40 THz. The demonstrated tuning bandwidth was limited by the detection scheme and the optical coatings used for combining the different frequency components of the generating beam. Fig. 7(b) shows the effect of the CEP locking of the laser pulse on the measured THz transient. In the case of a free running laser a THz pulse is generated by every laser pulse, but due to random phase of the THz pulse the average signal measured with our field sensitive electro optic (EO) sampling detection setup is zero.

6. Mapping of electric current with ATI spectroscopy

In addition to the optical detection described in the previous sections, the induced directional current induced by asymmetric field composed of incommensurate frequencies was also measured directly using electron spectrometry. Combination of several colors provides additional knobs to control the dynamics of sub-cycle ionization. This approach was successfully applied, for example, for the measurement of electron birth time in the HHG process [21] and isolated attosecond pulse generation [22,23]. Here we extend this approach and combine incommensurate frequency infrared colors to control the timing and the trajectory of the electron in a continuum.

In this section ATI electron spectroscopy measurements in xenon using intense two-color laser pulses are presented. A two color beam that is composed of a strong 1030 nm and a weaker 1545 nm signal wave is focused into a xenon gas cell. The intensity of approximately 0.6×10^{14} W/cm^2 is reached in the focus which corresponds to the regime where TI is a dominant process ($\gamma \approx 0.8$). In the strong field regime the electron wave packet evolution in the continuum is mainly determined by the shape of the laser field and the Coulomb interaction with the parent ion can be neglected.

The superposition of two colors can be considered as a train of few-cycle pulses with a DC offset (if the amplitudes of the two fields are not equal). In case of equal amplitudes of two colors E_1 and E_2, the resulting field is:

$$E = f(t)2\sin\left(\frac{\omega_1 + \omega_2}{2}t + \varphi_{CEP} + \frac{\varphi_{rel}}{2}\right)\cos\left(\frac{\omega_1 - \omega_2}{2}t - \frac{\varphi_{rel}}{2}\right)$$

(10)

In the case of combination of pulses with a wavelength of 1030 nm and 1545 nm, the synthesized field can be considered as a train of pulses with the corresponding carrier wavelength $\lambda = 4\pi c/(\omega_1 + \omega_2) = 1.2$ μm and separated by $T = 2\pi/(\omega_1 - \omega_2) = 10$ fs in time.

The experimental results are summarized in Fig. 8. The electron spectrum and a lineout at 15 eV shown in panels (a) and (b) are highly dependent on the CEP of the laser pulse. The electron asymmetry modulation depth at 15 eV exceeds 50%, which indicates good reproducibility of the generated waveforms. The calculated asymmetry map depicted in Fig. 8(c) shows the value of the normalized asymmetry parameter $a = (L - R)/(L + R)$ versus energy and CEP of the laser pulse. From this data the phase ellipse is obtained by taking lineouts at two different energy windows [24,25], which can be used for in situ calibration of the actual produced waveform.

Usually for the measurement of the CEP value the high energy part of the spectrum corresponding to rescattered electrons is used. The low energy part of the spectrum which is dominated by direct electrons, is also sensitive to the CEP of the pulse. Here we show that the CEP can be measured in situ not only from the

high energy part of the electron spectrum, but also using the low energy direct electrons to retrieve the CEP without π-ambiguity. From the experimental data in Fig. 9 a low energy window can be observed where the phase of the retrieved asymmetry varies with electron energy, allowing CEP retrieval without π ambiguity. The advantage of using low energy electrons over using high energy electrons is that the electron yield much higher allowing for low noise CEP detection without using very high gas densities. Another advantage of using low energy electrons is the better spectral resolusion of time of flight spectrometers at lower energies.

7. Conclusions

We have demonstrated that TI induces attosecond electron bursts that result in emission of new optical signals both at frequencies higher than the ionizing field and at frequencies lower than the ionizing field. In contrast to other attosecond metrology methods, the induced emission can be studied both in gases and bulk dielectrics. The experimental data are in good agreement with a calculations based on the semiclassical model describing ionization in the strong field regime and subsequent motion of the free electrons.

Acknowledgments

References

[1] L. Keldysh, Sov. Phys. JETP 20 (1965) 1307.
[2] G. Yudin, M. Ivanov, Phys. Rev. A 64 (2001) 013409.
[3] M. Uiberacker, Th. Uphues, M. Schultze, A. Verhoef, V. Yakovlev, M. Kling, J. Rauschenberger, N. Kabachnik, H. Schroder, M. Lezius, K. Kompa, H.-G. Muller, M. Vrakking, S. Hendel, U. Kleineberg, U. Heinzmann, M. Drescher, F. Krausz, Nature 446 (2007) 627.
[4] E. Goulielmakis, V. Yakovlev, A. Cavalieri, M. Uiberacker, V. Pervak, A. Apolonski, R. Kienberger, U. Kleineberg, F. Krausz, Science 317 (2007) 769.
[5] P. Corkum, F. Krausz, Nature Phys. 3 (2007) 381.
[6] Th. Uphues, M. Schultze, M. Kling1, M. Uiberacker, S. Hendel, U. Heinzmann, N. Kabachnik, M. Drescher, New J. Phys. 10 (2008) 025009. 2008.
[7] A. Cavalieri, N. Muller, Th. Uphues, V. Yakovlev, A. Baltuska, B. Horvath, B. Schmidt, L. Blumel, R. Holzwarth, S. Hendel, M. Drescher, U. Kleineberg, P. Echenique, R. Kienberger, F. Krausz, U. Heinzmann, Nature 449 (2007) 1029.
[8] A. Verhoef, A. Mitrofanov, E. Serebryannikov, D. Kartashov, A. Zheltikov, A. Baltuska, Phys. Rev. Lett. 104 (2010) 163904.
[9] F. Brunel, J. Opt. Soc. Am. B 7 (1990) 521.
[10] P. Corkum, Phys. Rev. Lett. 71 (1993) 1994.
[11] J. Mauritsson, P. Johnsson, E. Gustafsson, A. L'Huillier, K.J. Schafer, M.B. Gaarde, Phys. Rev. Lett. 97 (2006) 013001.
[12] M. Kress, T. Löffler, S. Eden, M. Thomson, H.G. Roskos, Opt. Lett. 29 (2004) 1120.
[13] K.Y. Kim, A.J. Taylor, J.H. Glownia, G. Rodriguez, Nat. Photonics 2 (2008) 605.
[14] N. Karpowicz, X.-C. Zhang, Phys. Rev. Lett. 102 (2009) 093001.
[15] Z. Zhou, D. Zhang, Z. Zhao, J. Yuan, Phys. Rev. A 79 (2009) 063413.
[16] M.V. Amosov, N.B. Delone, V.P. Krainov, Zh. Eksp, Teor. Fiz. 91 (1986) 2008.
[17] M. Gertsvolf, M. Spanner, D. Rayner, P. Corkum, J. Phys. B 43 (2010) 131002.
[18] C. Siders, G. Rodriguez, J.L.W. Siders, F.G. Omenetto, A.J. Taylor, Phys. Rev. Lett. 87 (2001) 263002.
[19] D.J. Cook, R.M. Hochstrasser, Opt. Lett. 25 (2000) 1210.
[20] T. Balčiūnas, D. Lorenc, M. Ivanov, O. Smirnova, A. Pugžlys, A. M. Zheltikov, D. Dietze, J. Darmo, K. Unterrainer, T. Rathje, G. G. Paulus, and A. Baltuška, in Proceedings of the 17th Int. Conference on Ultrafast Phenomena, 2010, p. 658.
[21] N. Dudovich, O. Smirnova, J. Levesque, Y. Mairesse, M.Yu. Ivanov, D.M. Villeneuve, P.B. Corkum, Nat. Phys. 2 (2006) 781.
[22] E.J. Takahashi, P. Lan, O.D. Mücke, Y. Nabekawa, K. Midorikawa, PRL 104 (2010) 233901.
[23] F. Calegari, C. Vozzi, M. Negro, G. Sansone, F. Frassetto, L. Poletto, P. Villoresi, M. Nisoli, S. De Silvestri, S. Stagira, Opt. Lett. 34 (2009) 3125.
[24] D. Milošević, G. Paulus, W. Becker, Opt. Express 11 (2003) 1418.
[25] T. Wittmann, B. Horvath, W. Helml, M.G. Schätzel, X. Gu, A.L. Cavalieri, G.G. Paulus, R. Kienberger, Nat. Phys. 5 (2009) 357.